Geophysical Research Letters

Radial Evolution of a CIR: Observations From a Nearly Radially Aligned Event Between Parker Solar Probe and STEREO-A

R. C. Allen[1] , G. C. Ho[1] , G. M. Mason[1] , G. Li[2] , L. K. Jian[3] , S. K. Vines[1] ,
N. A. Schwadron[4] , C. J. Joyce[5] , S. D. Bale[6,7,8,9] , J. W. Bonnell[7] , A. W. Case[10] ,
E. R. Christian[3] , C. M. S. Cohen[11] , M. I. Desai[12] , R. Filwett[13] , K. Goetz[14] ,
P. R. Harvey[7] , M. E. Hill[1] , J. C. Kasper[10,15] , K. E. Korreck[10] , D. Lario[3] ,
D. Larson[7] , R. Livi[7] , R. J. MacDowall[3] , D. M. Malaspina[16] , D. J. McComas[5] ,
R. McNutt[1] , D. G. Mitchell[1] , K. W. Paulson[10] , M. Pulupa[7] , N. Raouafi[1] ,
M. L. Stevens[10] , P. L. Whittlesey[7] , and M. Wiedenbeck[17]

[1]Johns Hopkins University, Applied Physics Lab, Laurel, MD, USA, [2]Department of Space Science, University of Alabama in Huntsville, Huntsville, AL, USA, [3]Heliospheric Physics Laboratory (Code 672), NASA/Goddard Space Flight Center, Greenbelt, MD, USA, [4]Space Science Center, University of New Hampshire, Durham, NH, USA, [5]Department of Astrophysical Science, Princeton University, Princeton, NH, USA, [6]Physics Department, University of California, Berkeley, CA, USA, [7]Space Sciences Laboratory, University of California, Berkeley, CA, USA, [8]The Blackett Laboratory, Imperial College London, London, UK, [9]School of Physics and Astronomy, Queen Mary University of London, London, UK, [10]Smithsonian Astrophysical Observatory, Cambridge, MA, USA, [11]Space Radiation Laboratory, California Institute of Technology, Pasadena, CA, USA, [12]Space Science and Engineering Division, Southwest Research Institute, San Antonio, TX, USA, [13]Department of Physics and Astronomy, University of Iowa, Iowa City, IA, USA, [14]School of Physics and Astronomy, University of Minnesota, Minneapolis, MN, USA, [15]Climate and Space Sciences and Engineering, University of Michigan, Ann Arbor, MI, USA, [16]Laboratory for Atmospheric and Space Physics, University of Colorado, Boulder, CO, USA, [17]Jet Propulsion Laboratory, California Institute of Technology, Pasadena, CA, USA

Abstract The addition of Parker Solar Probe (PSP) to the Heliophysics System Observatory has allowed for the unprecedented ability to study Corotating Interaction Regions (CIRs) at multiple radial distances without significant temporal/longitudinal variations. On September 19, 2019, PSP observed a CIR at ∼0.5 au when it was nearly radially aligned with the Solar Terrestrial Relations Observatory-Ahead (STEREO-A) spacecraft at ∼1 au, allowing for an unambiguous assessment of the radial evolution of a single CIR. Bulk plasma and magnetic field signatures of the CIR evolve in a fashion characteristic to previous observations; however, the suprathermal ions are enhanced over a larger longitudinal range at PSP than at STEREO-A, although at much lower intensities. The longitudinal spread appears to be largely a consequence of magnetic field line topology at CIRs between the compressed slow solar wind upstream and high-speed stream following the CIR, underscoring the importance of the large-scale topology of these structures.

1. Introduction

Corotating Interaction Regions (CIRs) form where corotating high-speed streams, originating from coronal holes, overtake slower-speed solar wind (Belcher & Davis, 1971; for a recent review, see Richardson, 2018). As the solar wind flows radially outward, forward, and reverse shocks can form along the CIR, often beyond 1 au (e.g., Jian et al., 2006, 2008; Pizzo, 1978; Smith & Wolfe, 1976), which serve as a significant source of energetic particles in the interplanetary medium (Tsurutani et al., 1982; van Hollebeke et al., 1981). While shock acceleration has historically been viewed as a main acceleration mechanism at CIRs, some studies have indicated the importance of particle acceleration mechanisms within 1 au such as stochastic processes (e.g., Chotoo et al., 2000; Richardson, 1985; Schwadron et al., 1996) or processes in the unshocked compression region due to the velocity gradient across the CIR (e.g., Chen et al., 2015; Ebert et al., 2012; Filwett et al., 2017; Giacalone et al., 2002).

The Helios 1 and 2 missions, launched in 1974 and 1976, respectively, allowed the ability to probe CIRs in the inner heliosphere for the first time. To better understand how CIRs evolve with radial distance, Richter and Luttrell (1986) performed a superposed epoch analysis using 16 CIRs between 0.3 and 0.4 au,

and 31 CIRs between 0.9 and 1.0 au. They found that the density, temperature, pressure, and magnetic field increase at the CIR interface increased with increasing radial distance. The azimuthal variation in the solar wind velocity profile also steepened with increasing distance. Other studies of near radially aligned CIR observations between the Helios spacecraft also found this velocity steepening and increased compression along the CIR interface (see Balogh et al., 1999; Forsyth & Marsch, 1999). While these studies illustrate the evolution of the CIR structure with distance due to the increasing inclination of the Parker spiral with respect to the radial direction, other studies have found the opposite correlations. Statistical results by Schwenn (1990), e.g., reported a decrease in the longitudinal speed gradients at the leading edge of CIRs from 0.3 to 0.5 au, attributing this to the sharp speed gradients at the boundaries of coronal holes, before becoming relatively unchanged from 0.5 to 1 au. Comparisons between Pioneer, Venus Orbiter, and Advanced Composition Explorer (ACE)/wind have also allowed for insight into the average variation of CIR characteristics between 0.72 and 1 au (Jian et al., 2008), finding little change in the velocity variation between these observations. However, very few events have been recorded by spacecraft at different radial distances but with the same longitude. As such, while changes in the average CIR profile by radial distance have been studied, though resulting in different trends at times, how individual CIRs evolve with radial distance is still largely unknown.

In addition to radial evolution, CIRs also evolve in time, longitude, and latitude. From one solar rotation to the next, the observed bulk plasma properties and the suprathermal particle intensities in CIRs change with time (e.g., Mason et al., 2009). Even when observed in close enough proximity, the suprathermal ion flux and spectra can be different between observations. Several studies have suggested this difference could be a result of successive observations being magnetically connected to a shock front at increasingly further distances, allowing for increasingly larger amounts of acceleration (e.g., Barnes & Simpson, 1976; Simnett & Roelof, 1995; Wijsen et al., 2019; Zhao et al., 2015). Beyond single CIR observations, solar cycle variations have also been observed in CIR occurrence and properties (Jian et al., 2011, 2019) and in their suprathermal ion composition (Allen et al., 2019; Filwett et al., 2017; Mason et al., 2008, 2012). As such, inferences from combining all CIR observations from many different points in time may not accurately represent any single constituent event. In the modern era of the Heliophysics System Observatory, Parker Solar Probe (PSP), in combination with observations at 1 au, allows for an unprecedented opportunity to disentangle the radial and temporal evolution of CIRs. During the first orbit of PSP, several studies investigated CIRs in the inner heliosphere (Allen et al., 2020a; Cohen et al., 2020; Desai et al., 2020; Joyce et al., 2020; McComas et al., 2019). Allen et al. (2020a) matched CIRs observed at PSP during its first orbit with observations at 1 au from the Solar Terrestrial Relations Observatory-Ahead (STEREO-A), ACE, and wind missions. While this provided insight into possible differences in the energization of suprathermal ions in the inner heliosphere and their connectivity to shocks further out in the heliosphere, the conjunction geometry did not allow for the ability to differentiate between temporal and radial evolution.

In this study, we investigate a conjunction between PSP and STEREO-A, when the two spacecraft were nearly radially aligned. This allows for a comparison of the radial evolution of a CIR without the uncertainties arising from effects of significant temporal evolution. Section 2 describes the data sets used, the results of which are presented in Section 3. Discussion and summary of the conclusions of this work are given in Sections 4 and 5, respectively.

2. Missions and Data Sets

2.1. Parker Solar Probe

The PSP mission (Fox et al., 2016) was launched into a heliocentric orbit around the Sun on August 12, 2018. This study uses 1-min averages of bulk solar wind measurements from the Solar Probe Cup (SPC; Case et al., 2020), part of the Solar Wind Electrons Alpha and Protons (SWEAP) instrument suite (Kasper et al., 2016). Magnetic field measurements are provided by the FIELDS suite (Bale et al., 2016), and are averaged into a 1-min resolution product. This study computes proton temperature (T), specific entropy argument (S), and the combined proton plasma and magnetic pressure (P) following the methodology outlined in Allen et al. (2020a). Suprathermal ion measurements from the Energetic Particle Instrument-Lo (EPI-Lo; Hill et al., 2017), part of the Integrated Science Investigation of the Sun (ISʘIS; McComas et al., 2016), are averaged to a 30-min resolution data set.

2.2. STEREO-A

The STEREO mission (Kaiser et al., 2008) is a set of two spacecraft that were launched on October 25, 2006, and sent to orbit the Sun in opposing directions when viewed in a Sun-Earth fixed frame. This study focuses on observations by STEREO-A (STA) and uses 1-min averaged magnetic field observations from the magnetometer (Acuña et al., 2008), along with suprathermal particle measurements from the Solar Electron and Proton Telescope (SEPT; Müller-Mellin et al., 2008) instrument, both part of the In situ Measurements of Particles and CME Transients (IMPACT) investigation (Luhmann et al., 2008). SEPT is able to measure ions, but cannot differentiate ion species, so these ions are assumed to predominantly be H⁺. Additionally, 1-min bulk solar wind properties (i.e., velocity, temperature, and density) are provided by the Plasma and Suprathermal Ion Composition (PLASTIC) investigation (Galvin et al., 2008).

2.3. Wind

For comparison to STEREO-A, data from the wind mission (Acuña et al., 1995) are also presented. Wind was launched on November 1, 1994 and has been stationed at L1 since 2004. 1-min resolution bulk solar wind plasma properties, from the Solar Wind Experiment (SWE; Ogilvie et al., 1995), and magnetic field measurements, from the Magnetic Field Instrument (MFI; Lepping et al., 1995), are used in this study.

3. Results

3.1. Observations at 1 au

A CIR was observed at 1 au by STA and wind (~84° in longitude apart) during solar rotations prior to and after the observation of the CIR at PSP at 0.51 au on September 19, 2019. Figure 1 shows plasma, magnetic field, and suprathermal particle observations at 1 au for this CIR. These observations are time-shifted such that the individual interfaces all line up with that of the third STA observation, denoted by the vertical dashed line in Figure 1. With each successive observation (comparing the dark blue and red traces in Figures 1a–1h, in particular), the velocity increase becomes steeper, the density pileup becomes more pronounced, and the increases in temperature and entropy also steepen. Additionally, the suprathermal ion enhancement seen by STA (Figures 1i–1k) becomes more intense. These variations between successive observations highlight the various ways in which long-lived CIRs can evolve in time.

3.2. Radial Evolution

During the third STA observation of this CIR (STA E3 in Figure 1), STA and PSP were nearly radially aligned (within 4.2° longitude and 0.26° latitude when the CIR passed over PSP on September 19, 2019), with PSP at ~0.5 au (~80° in longitude from L1) and STA at 0.98 au. To compare the solar wind and IMF observations at different radial distances (r), approximate scaling laws (see Kivelson & Russell, 1995) were applied to the STA data set: $n \propto r^{-2}$, $T \propto r^{-4/3}$, $B_r \propto r^{-2}$, and $B_t \propto r^{-1}$, where B_r and B_t denote the radial and tangential components of the interplanetary magnetic field (IMF) in radial-tangential-normal (RTN) coordinates. These scalings are applied to remove the underlying systematic radial variations, such as from volumetric expansion, to highlight the variations caused by the interaction between the slow and high-speed streams. Figure 2 illustrates the PSP observations (in black) and the scaled STA observations (in blue) that are also shifted in time by −1.77 days to align the CIR interfaces (as determined by eye). This shift is consistent with corotation after taking into account the different radial distances. The velocity, density, temperature, entropy, pressure, and magnetic field observations at PSP and the radially scaled STA E3 observations are in remarkable agreement, suggesting very little temporal variation between the observations. Focusing on the transition from slow to fast solar wind, the density pileup and pressure enhancement are more pronounced at STA than at PSP, although comparisons of the velocity, temperature, entropy, and magnetic field strength are difficult to fully assess due to data gaps during the interval at PSP (to conserve power, the instruments are powered off during scheduled high-rate Ka-band downlink opportunities). While both PSP and STA are within 0.26° of each other in heliographic latitude, STA likely observed the CIR closer to the heliospheric current sheet (HCS) than PSP (as apparent in the abrupt change in ϕ_{RTN} observed just before the CIR; Figure 2h). Additionally, a suprathermal ion flux enhancement associated with the CIR was observed at both
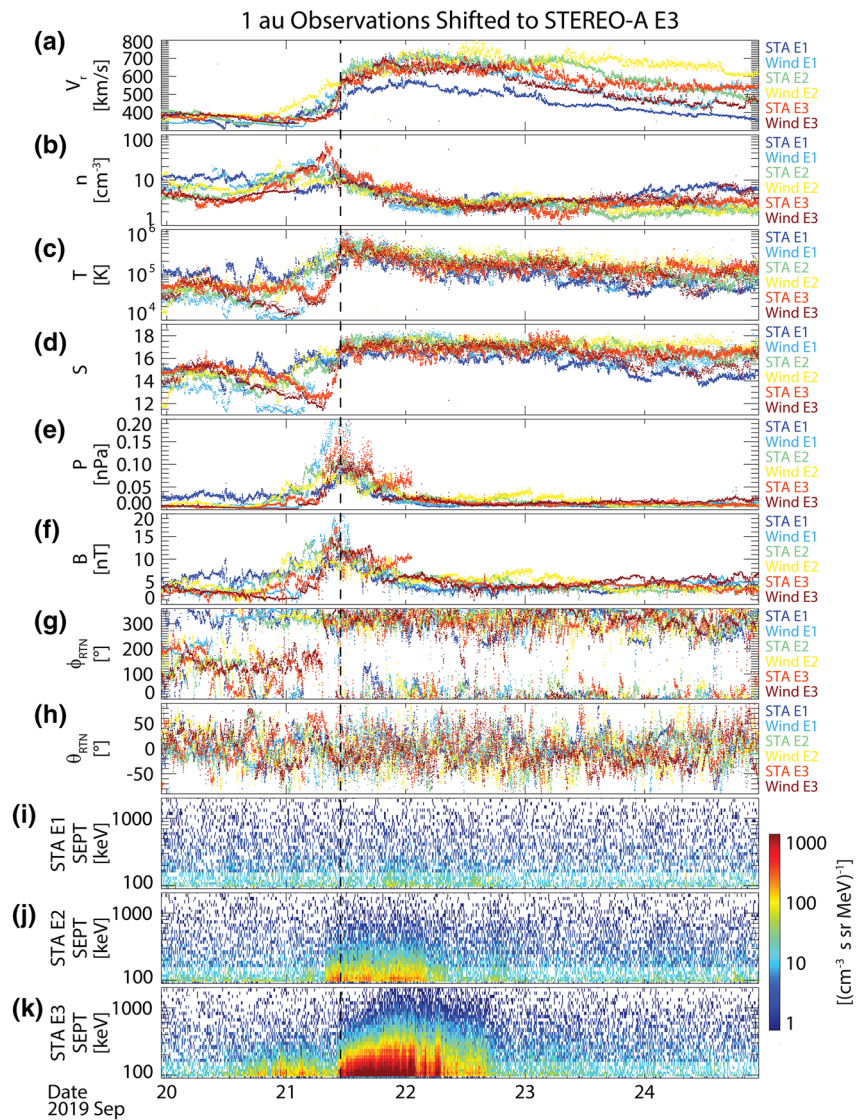
Figure 1. Observations of a CIR at 1 au from STA and wind time-shifted to match the stream interface of the STA event 3 (E3) (vertical dashed line). The CIR interface, identified as the time of peak pressure of the CIR (e.g., Jian et al., 2006), occurred at July 30, 2019/19:33:30 (labeled STA E1), August 5, 2019/08:01:30 (Wind E1), August 25, 2019/05:05:30 (STA E2), August 31, 2019/01:06:30 (Wind E2), September 21, 2019/10:55:30 (STA E3), and September 27, 2019/13:54:30 (Wind E3). From top to bottom, (a) radial velocity, (b) density, (c) temperature, (d) entropy, (e) combined proton and magnetic field pressure, (f) magnetic field magnitude, magnetic field (g) ϕ_{RTN} and (h) θ_{RTN} components in the RTN coordinate system, and (i)–(k) suprathermal ion intensity from SEPT on STA for the first, second, and third STA observations, respectively. CIR, Corotating Interaction Region; STA, STEREO-A; SEPT, Solar Electron and Proton Telescope.

PSP (Figure 2i) and STA (Figure 2j). The small enhancement at STA prior to the HCS crossing is likely un-related to the CIR (see, Smith et al., 1978). Notably, the suprathermal ion enhancement at PSP is observed for a longer duration, corresponding to a larger longitudinal extent, than at STA.

To further investigate the radial change of the suprathermal ion population, intensities over two time intervals, September 19, 2019/14:40–September 20, 2019/06:40 UT (defined to be within the main pressure enhancement of the CIR and denoted by the dotted vertical lines and green triangles) and September 20, 2019/14:00–September 21, 2019/02:00 UT (encompassing the time period in the high-speed stream with both PSP and STA suprathermal ion observations and denoted by the vertical dashed lines and green squares),
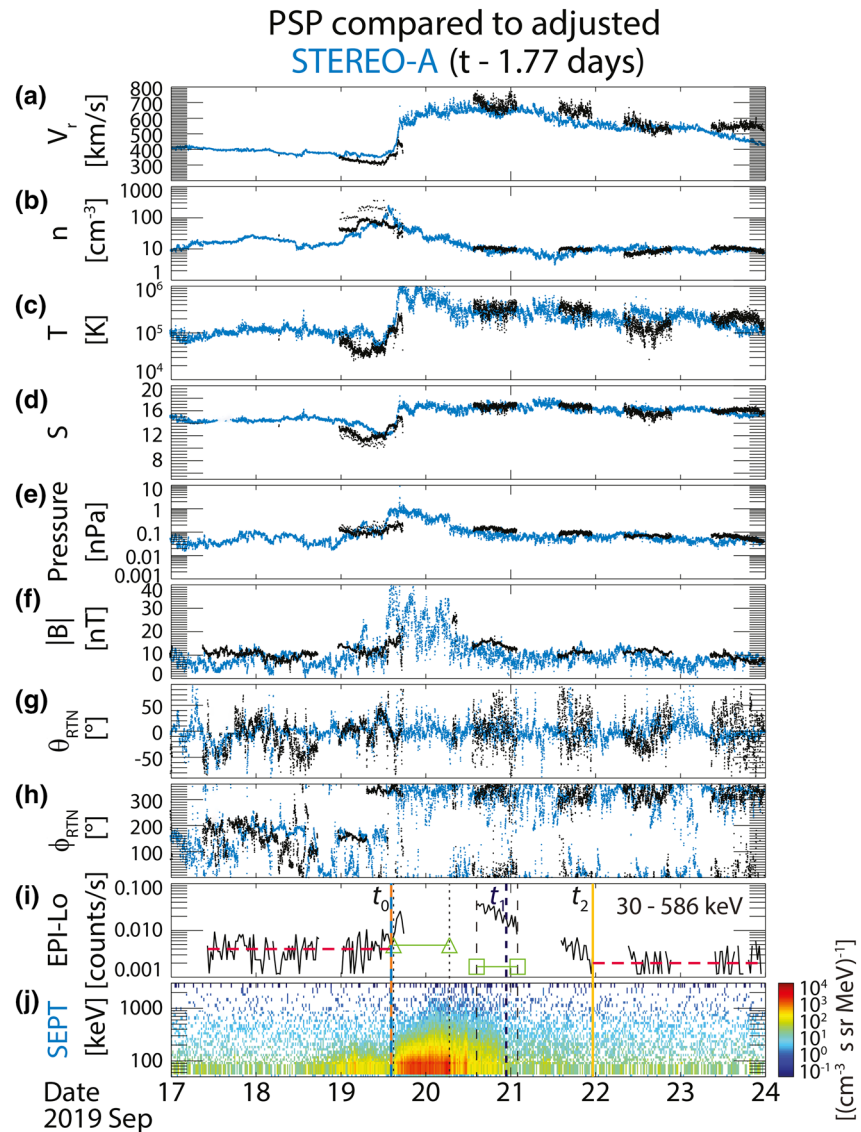
Figure 2. CIR observation at PSP (black) and STA (blue) for STA E3. The STA E3 observations are shifted in time by 1.77 days and are scaled according the relations provided in the text. From top to bottom, (a) radial velocity, (b) density, (c) temperature, (d) entropy, (e) combined proton and magnetic field pressure, (f) magnetic field magnitude, (g) ϕ_{RTN}, (h) θ_{RTN}, (i) PSP EPI-Lo "ToF only" mode count rate, and (j) STA SEPT flux spectrograms are shown. See text for description of markings on panels i and j, denoting intervals in Figures 3 and 4. CIR, Corotating Interaction Region; STA, STEREO-A; SEPT, Solar Electron and Proton Telescope; PSP, Parker Solar Probe.

were averaged to construct ion spectra. Due to the data gaps at PSP, EPI-Lo observations are only shown for the second timeframe. Figure 3 displays these spectra with STA SEPT observations (green), PSP H^+ (red), and PSP $^4He^{n+}$ (blue). Power law fits were applied for energies <1,000 keV/nuc for STA and <600 keV/nuc for PSP. The enhancement in suprathermal ion flux for PSP H^+ above 600 keV is related to known cross-talk background in the instrument (see Hill et al., 2020), and is ignored in our analysis.

Comparing the STA ion power law within the CIR (triangles) to those later in the high-speed stream (squares), the power law hardens slightly through the event (−3.1 to −2.5, respectively). While the power law indices are nearly the same between PSP and the later STA interval (−2.5), the intensity of the suprathermal ion enhancement at PSP is significantly lower by a factor of ∼40 (i.e., red vs. green squares in Figure 3).
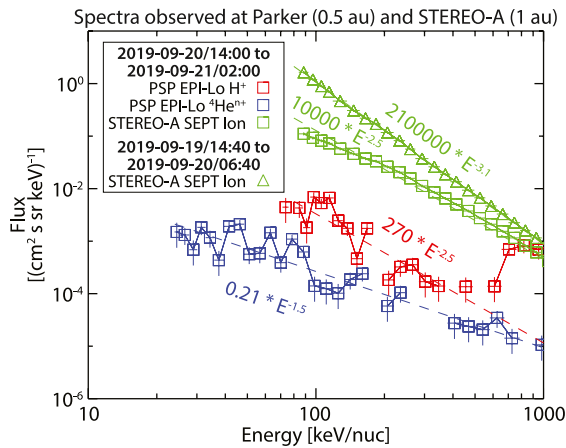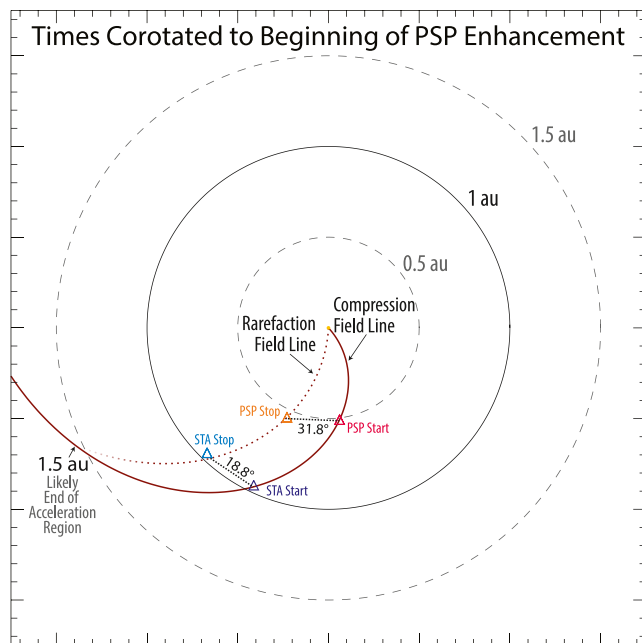
Figure 3. Flux spectra for suprathermal $^4He^{n+}$ (blue) and H^+ (red) observed at PSP, and total ions (green) observed at STA for a subinterval inside the CIR structure (triangles) and within the trailing high-speed stream (squares) where both STA and PSP have measurements available. CIR, Corotating Interaction Region; STA, STEREO-A; PSP, Parker Solar Probe.

3.3. Longitudinal Spread of Energetic Particles

To further investigate the longitudinal spread of the suprathermal ion enhancement at PSP vs. that at STA, we define start and stop times of the enhancements for both observations. Red horizontal dashed lines in Figure 2i mark the average EPI-Lo count rates before and after the suprathermal ion enhancement at PSP. The time that the EPI-Lo count rate exceeds the averaged preevent background count rate is considered the start time (t_0 = September 19, 2019/14:00 UT, shown by the orange vertical dashed line in Figures 2i and 2j). Using a similar method, the time-shifted STA SEPT flux was found to become enhanced at the same time (in the shifted timeframe). The time the STA count rate reached the postevent average rate was defined as the STA enhancement stop time (t_1 = September 20, 2019/22:20 UT, shown by the thick vertical dashed line in Figures 2i and 2j). This method also identified the PSP enhancement stop time (t_2, shown as the solid yellow vertical lines in Figures 2i and 2j) at September 21, 2019/23:30 UT. Comparing the times of the suprathermal ion enhancements at STA to the bulk plasma properties during this interval, the enhancements begins near the CIR interface. Additionally, there is a decrease in the suprathermal ion intensity near the trailing edge of the CIR at STA; however, the intensity remains elevated into the high-speed stream. Due to data gaps in the PSP observations, we cannot reliably compare the energetic particle enhancements at PSP to the bulk plasma structure of the CIR in the same fashion.

To further examine the role of the underlying IMF structure in the longitudinal spread of the energetic particles, Parker spiral IMF lines were computed using the solar wind velocity observed by PSP at the beginning and end of the suprathermal ion enhancements (t_0 and t_2 computed above). The Parker spiral IMF line corresponding to the end of the suprathermal ion enhancement at PSP was then corotated backward to correspond to its location at the start of the ion enhancement (t_0). For both the Parker spiral calculations and corotation distance, a fixed corotation speed of 14.7°/day was used, consistent with the equatorial corotation speed of the Sun. Using a wider range of corotation speeds that have been previously observed for CIRs (13.4°/day–14.7°/day, cf. Allen et al., 2020b) yielded similar results (not shown). The two Parker spiral IMF lines are shown in Figure 4, with the "compression field line" denoting the Parker spiral based on observations at the start of the ion enhancement at PSP (t_0), and the "rarefaction field line" denoting the corotated Parker spiral in the fast solar wind when the suprathermal ion flux returned to the background level (t_2).

Figure 4. Parker spiral field lines calculated from PSP observations at the start and stop times of the suprathermal ion enhancements are shown by the solid and dotted maroon lines, respectively. The start and stop location of the PSP and STA suprathermal ion enhancements (triangles) are corotated to the beginning of the PSP enhancement. STA, STEREO-A; PSP, Parker Solar Probe.

Taking the start/stop times of the suprathermal ion enhancements at both PSP and STA, we compute the time difference between those times and t_0. Using this time difference and a fixed corotation speed (14.7°/day), we corotate the locations of PSP and STA observations to the reference time t_0, resulting in the labeled triangles in Figure 4. These locations are seen to largely agree with the Parker spiral field lines. Due to the rarefaction field line being more radial than the compression field line, arising from the different solar wind speeds at those times, the different curvatures lead to variable longitudinal spreads. For this event, the longitudinal spread at the radial distance of PSP was 31.8°, while the longitudinal spread at STA was only 18.8°. While it is known that the interaction between slow and fast streams can cause the magnetic topology to deviate from a Parker spiral configuration, this coarse approximation over smaller distances (0.5 au in this case) is found to be appropriate in aligning these observations. Although the zeroth-order treatment here

aligns the timing of the observations quite well, small variations are observed which could be an effect of higher-order corrections to the Parker spiral and/or differences in instrument sensitivities. The compression and rarefaction field lines approach each other at a distance of ~1.5 au, suggesting the CIR-associated acceleration processes are occurring within this distance, and so allowing the suprathermal particles access to the flux tube constrained by these field lines.

4. Discussion and Summary

This study explores a unique and fortuitous CIR event when PSP and STA were nearly radially aligned. Additionally, we examined the variations of this CIR over several solar rotations as seen by STA and wind. At 1 au, the CIR structure persisted for three solar rotations and shows a clear temporal evolution from one observation to the next (Figure 1). The third STA observation of the CIR occurred when STA and PSP were nearly radially aligned. Shifting the STA E3 measurements earlier in time by 1.77 days temporally aligned the observations between PSP and STA. Scaling the STA plasma and fields measurements by theoretical radial dependencies aligned the observations remarkably, suggesting little temporal evolution between observations at PSP and the third STA observation of this CIR (Figure 2).

Examining the suprathermal ion energy spectra associated with the CIR observed at PSP, the $^4\text{He}^{n+}$ spectral slope is harder than for H^+ (−1.5 to −2.5, respectively). This is often observed for CIRs at and beyond 1 au, and is thought to be an effect of preferential acceleration of pick up ions at CIRs, possibly indicating acceleration within 1 au (e.g., Chotoo et al., 2000; Gloeckler & Geiss, 1998; Gloeckler et al., 1994; Schwadron et al., 1996). Future studies probing how the spectral slopes for helium ions as compared to protons vary with radial distance can give further insight into species-dependent transport and acceleration processes. Looking at the full CIR interval at 1 au, the STA ion spectral slope evolves throughout event (noting the green triangles vs. the green squares in Figure 3). This evolution in the spectral slopes is likely associated with the spectra being taken inside vs. outside of the CIR structure (e.g., Barnes & Simpson, 1976). When observations exist for both spacecraft toward the latter half of the suprathermal ion enhancement, the spectral indices of ions at STA and H^+ at PSP are approximately the same (~2.5; green and red squares for STA and PSP, respectively, in Figure 3).

Under the assumption that the main source of particle acceleration is at heliocentric distances beyond both spacecraft, transport processes undergone by the particles would typically be invoked to explain lower particle intensities with decreasing heliocentric distances. While the suprathermal H^+ intensities are ~40 times lower at PSP than STA during the time period following the CIR interface when both spacecraft have data, the spectral profiles at both spacecraft have the same slope. Because these processes are also predicted to manifest themselves as an increasingly hardened spectra at lower energies with distance from the source region (e.g., Fisk & Lee, 1980), but no such hardening is observed in this event, this points to far weaker modulation of energetic particles than expected, as also indicated by other studies (e.g., Desai et al., 2020; Mason & Sanderson, 1999; Mason et al., 2008, 2012, 1997; Schwadron et al., 2020).

While the suprathermal ion enhancement at PSP is observed over a longer time period and longitudinal range than that seen for STA, this can be explained due to the geometry of the magnetic field lines (Figure 4). For this event, the suprathermal ion enhancement at both PSP and STA begin in the compressed slow solar wind and end in the rarefaction region high-speed stream (Figure 2). As a result of the difference in solar wind speed, the Parker spiral field line in the high-speed stream is more radial than that of the compressed slow solar wind. This difference in Parker spiral geometry results in a radial dependence to the longitudinal extent of the flux tube. For this event, this corresponds to a longitudinal extent of 18.8° and 31.8° at the radial distance of STA and PSP, respectively, consistent with the observations. Under the assumption that the particles were accelerated at larger heliospheric distances, the width of the suprathermal ion enhancements suggests acceleration occurred within ~1.5 au. Since STA did not observe a shock at 1 au, but only a developing reverse shock, it is not clear if a shock became fully formed at slightly further heliospheric distances, or if instead compressive acceleration is resulting in the observed suprathermal particles through stochastic processes and/or mechanisms occurring in the unshocked compression region due the velocity gradient across the CIR, similar to diffusive shock acceleration at a quasi-parallel shock (e.g., Chen et al., 2015; Chotoo et al., 2000; Ebert et al., 2012; Filwett et al., 2017; Giacalone et al., 2002; Joyce

et al., 2020; Richardson, 1985). Due to the close proximity to the acceleration region estimated for this event (within 1.5 au), the Parker spiral approximation for the magnetic field topology well describes the general structuring of this CIR event to zeroth-order. However, determining the topology of CIR events in which acceleration occurs at larger heliospheric distances would require more detailed mapping due to sub-Parker spiral field lines (e.g., Murphy et al., 2002; Schwadron, 2002; Schwadron & McComas, 2005, Schwadron et al., 2020) and the interaction between the slow and fast solar wind along the CIR interface. Further investigation of other events between PSP and other observatories can be used to better understand the transport of suprathermal particles into the inner heliosphere. Additionally, future conjunctions between PSP, STA, wind, and Solar Orbiter will allow for continued investigation into the variations of CIRs with radial distance, longitude, and latitude.

Data Availability Statement

Parker Solar Probe data can be accessed from https://sppgway.jhuapl.edu/. The STEREO SEPT data are available at http://www2.physik.uni-kiel.de/stereo/data/sept/, and STEREO magnetic field and plasma data can be found at the STEREO Science Center: https://stereo-ssc.nascom.nasa.gov. Wind data are available at https://cdaweb.gsfc.nasa.gov/. This event is taken from the catalog by Allen et al. (2020c).

References

Acuña, M. H., Curtis, D., Scheifele, J. L., Russell, C. T., Schroeder, O., Szabo, A., & Luhmann, J. G. (2008). The STEREO/IMPACT magnetic field experiment. *Space Science Reviews*, *136*, 203–226. https://doi.org/10.1007/s11214-007-9259-2

Acuña, M. H., Ogilvie, K. W., Baker, D. N., Curtis, S. A., Fairfield, D. H., & Mish, W. H. (1995). The global geospace science program and its investigations. *Space Science Reviews*, *71*, 5–21. https://doi.org/10.1007/BF00751323

Allen, R. C., Ho, G. C., Jian, L. K., Mason, G. M., Vines, S. K., & Lario, D. (2020a). Predictive capabilities and limitations of stream interaction region observations at different solar longitudes. *Space Weather*, *18*, e2019SW002437. https://doi.org/10.1029/2019SW002437

Allen, R. C., Ho, G. C., Jian, L. K., Vines, S. K., Bale, S. D., Case, A., et al. (2020b). A living catalog of stream interaction regions in the Parker Solar Probe era. *Astronomy and Astrophysics.* https://doi.org/10.1051/0004-6361/202039833

Allen, R. C., Ho, G. C., & Mason, G. M. (2019). Suprathermal ion abundance variations in corotating interactions regions over two solar cycles. *The Astrophysical Journal Letters*, *883*(1), L10. https://doi.org/10.3847/2041-8213/ab3f3f

Allen, R. C., Lario, D., Odstrcil, D., Ho, G. C., Jian, L. K., Cohen, C. M. S., et al. (2020c). Solar wind streams and stream interaction regions observed by the Parker Solar Probe with corresponding observations at 1 au. *The Astrophysical Journal Supplement*, *246*(2), 36. https://doi.org/10.3847/1538-4365/ab578f

Bale, S. D., Goetz, K., Harvey, P. R., Turin, P., Bonnell, J. W., Dudok de Wit, T., et al. (2016). The FIELDS instrument suite for Solar Probe Plus. Measuring the coronal plasma and magnetic field, plasma waves, and turbulence, and radio signatures of solar transients. *Space Science Reviews*, *204*, 49–82. https://doi.org/10.1007/s11214-016-0244-5

Balogh, A., Bothmer, V., Crooker, N. U., Forsyth, R. J., Gloeckler, G., Hewish, A., et al. (1999). The solar origin of corotating interactions regions and their formation in the inner heliosphere. *Space Science Reviews*, *89*, 141–178. https://doi.org/10.1023/A:1005245306874

Barnes, C. W., & Simpson, J. A. (1976). Evidence for interplanetary acceleration of nucleons in corotating interaction regions. *The Astrophysical Journal*, *210*, L91–L96.

Belcher, J. W., & Davis, L. (1971). Large-amplitude Alfvén waves in the interplanetary medium, 2. *Journal of Geophysical Research*, *76*, 3534–3563. https://doi.org/10.1029/JA076i016p03534

Case, A. W., Kasper, J. C., Stevens, M. L., Korreck, K. E., Paulson, K., Daigneau, P., et al. (2020). The Solar Probe Cup on the Parker Solar Probe. *The Astrophysical Journal Supplement*, *246*(2), 43. https://doi.org/10.3847/1538-4365/ab5a7b

Chen, J. H., Schwadron, N. A., Möbius, E., & Gorby, M. (2015). Modeling interstellar pickup ion distributions in corotating interaction regions inside 1 au. *Journal of Geophysical Research: Space Physics*, *120*, 9269–9280. https://doi.org/10.1002/2014JA020939

Chotoo, K., Schwadron, N. A., Mason, G. M., Zurbuchen, T. H., Gloeckler, G., Posner, A., et al. (2000). The suprathermal seed population for corotating interaction region ions at 1 au deduced from composition and spectra of H^+, He^{++}, and He^+ observed on wind. *Journal of Geophysical Research*, *105*, 23107–23122. https://doi.org/10.1029/1998JA000015

Cohen, C. M. S., Christian, E. R., Cummings, A. C., Davis, A. J., Desai, , M. I., Giacalone, J., et al. (2020). Energetic particle increases associated with stream interaction regions. *The Astrophysical Journal Supplement*, *246*(2), 20. https://doi.org/10.3847/1538-4365/ab4c38

Desai, M. I., Mitchell, D. G., Szalay, J. R., Roelof, E. C., Giacalone, J., Hill, M. E., et al. (2020). Properties of suprathermal-through-energetic He ions associated with stream interaction regions observed over the Parker Solar Probe's first two orbits. *The Astrophysical Journal Supplement*, *246*(2), 56. https://doi.org/10.3847/1538-4365/ab65ef

Ebert, R. W., Dayeh, M. A., Desai, M. I., & Mason, G. M. (2012). Corotating interaction region associated suprathermal helium enhancements at 1 au: Evidence for local acceleration at the compression region trailing edge. *The Astrophysical Journal*, *749*, 73. https://doi.org/10.1088/0004-637X/749/1/73

Filwett, R. J., Desai, M. I., Dayeh, M. A., & Broiles, T. W. (2017). Source population and acceleration location of suprathermal heavy ions in corotating interaction regions. *The Astrophysical Journal*, *838*(1), 23. https://doi.org/10.3847/1538-4357/aa5ca9

Fisk, L. A., & Lee, M. A. (1980). Shock acceleration of energetic particles in corotating interaction regions in the solar wind. *The Astrophysical Journal*, *237*, 620–626. https://doi.org/10.1086/157907

Forsyth, R. J., & Marsch, E. (1999). Solar origin and interplanetary evolution of stream interfaces. *Space Science Reviews*, *89*, 7–20. https://doi.org/10.1023/A:1005235626013

Fox, N. J., Velli, M. C., Bale, S. D., Decker, R., Driesman, A., Howard, R. A., et al. (2016). The Solar Probe Plus Mission: Humanity's first visit to our star. *Space Science Reviews*, *204*, 7–48. https://doi.org/10.1007/s11214-015-0211-6

Galvin, A. B., Kistler, L. M., Popecki, M. A., Farrugia, C. J., Simunac, K. D. C., Ellis, L., et al. (2008). The Plasma and Suprathermal Ion Composition (PLASTIC) investigation on the STEREO observatories. *Space Science Reviews*, *136*(1), 437–486. https://doi.org/10.1007/s11214-007-9296-x

Giacalone, J., Jokipii, J. R., & Kóta, J. (2002). Particle acceleration in solar wind compression regions. *The Astrophysical Journal*, *573*(2), 845. https://doi.org/10.1086/340660

Gloeckler, G., & Geiss, J. (1998). Interstellar and inner source pickup ions observed with SWICS on Ulysses. *Space Science Reviews*, *85*, 127–159. https://doi.org/10.1023/A:1005019628054

Gloeckler, G., Geiss, J., Roelof, R. C., Fisk, L. A., Ipavich, F. M., Ogilvie, K. W., et al. (1994). Acceleration of interstellar pickup ions in the disturbed solar wind observed by Ulysses. *Journal of Geophysical Research*, *99*, 17637–17643. https://doi.org/10.1029/94JA01509

Hill, M. E., Mitchell, D. G., Andrews, G. B., Cooper, S. A., Gurnee, R. S., Hayes, J. R., et al. (2017). The mushroom: A half-sky energetic ion and electron detector. *Journal of Geophysical Research: Space Physics*, *122*, 1513–1530. https://doi.org/10.1002/2016JA022614

Hill, M. E, Mitchell, D. G., Allen, R. C., de Nolfo, G. A., Vourlidas, A., Brown, L. E., et al. (2020). Small, Low-energy, Dispersive Solar Energetic Particle Events Observed by Parker Solar Probe. *The Astrophysical Journal Supplement Series*, *246*(2), 65. https://doi.org/10.3847/1538-4365/ab643d

Jian, L., Russell, C. T., Luhmann, J. G., & Skoug, R. M. (2006). Properties of stream interaction at one AU during 1995–2004. *Solar Physics*, *239*, 337–392. https://doi.org/10.1007/s11207-006-0132-3

Jian, L. K., Luhmann, J. G., Russell, C. T., & Galvin, A. B. (2019). Solar Terrestrial Relations Observatory (STEREO) observations of stream interaction regions in 2007–2016: Relationship with heliospheric current sheets, solar cycle variations, and dual observations. *Solar Physics*, *294*, 31. https://doi.org/10.1007/s11207-019-1416-8

Jian, L. K., Russell, C. T., & Luhmann, J. G. (2011). Comparing solar minimum 23/24 with historical solar wind records at 1 AU. *Solar Physics*, *274*(1), 321–344. https://doi.org/10.1007/s11207-011-9737-2

Jian, L. K., Russell, C. T., Luhmann, J. G., Skoug, R. M., & Steinberg, J. T. (2008). Stream interaction and interplanetary coronal mass ejections at 5.3 AU near the solar ecliptic plane. *Solar Physics*, *250*, 375–402. https://doi.org/10.1007/s11207-008-9204-x

Joyce, C. J., McComas, D. J., Christian, E. R., Schwadron, N. A., Wiedenbeck, M. E., McNutt, R., et al. (2020). Energetic particle observations from the Parker Solar Probe using combined energy spectra from the ISOIS instrument suite. *Astrophysical Journal Supplement*, *246*, 41. https://doi.org/10.3847/1538-4365/ab5948

Kaiser, M. K., Kucera, T. A., Davila, J. M., Cyr, O. C. S., Guhathakurta, M., & Christian, E. (2008). The STEREO mission: An introduction. *Space Science Reviews*, *136*, 5–16. https://doi.org/10.1007/s11214-007-9277-0

Kasper, J. C., Abiad, R., Austin, G., Balat-Pichelin, M., Bale, S. D., Belcher, J. W., et al. (2016). Solar Wind Electrons Alphas and Protons (SWEAP) investigation: Design of the solar wind and coronal plasma instrument suite for Solar Probe Plus. *Space Science Reviews*, *204*, 131–186. https://doi.org/10.1007/s11214-015-0206-3

Kivelson, M. G., & Russell, C. T. (1995). *Introduction to space physics*. New York, NY: Cambridge University Press. IBSN: 9780521457149.

Lepping, R. P., Acuna, M. H., Burlaga, L. F., Farrell, W. M., Slavin, J. A., Schatten, K. H., et al. (1995). The wind magnetic field investigation. *Space Science Reviews*, *71*, 207–229. https://doi.org/10.1007/BF00751330

Luhmann, J. G., Curtis, D. W., Schroeder, P., McCauley, J., Lin, R. P., Larson, D. E., et al. (2008). STEREO IMPACT investigation goals, measurements, and data products overview. *Space Science Reviews*, *136*, 117–184. https://doi.org/10.1007/s11214-007-9170-x

Mason, G. M., Desai, M. I., & Li, G. (2012). Solar cycle abundance variations in corotating interaction regions: Evidence for a suprathermal ion seed population. *The Astrophysical Journal Letters*, *748*(2), L31. https://doi.org/10.1088/2041-8205/748/2/L31

Mason, G. M., Desai, M. I., Mall, U., Korth, A., Bucik, R., von Rosenvinge, T. T., et al. (2009). In situ observations if CIRs on STEREO, wind, and ACE during 2007-2008. *Solar Physics*, *256*, 393–408. https://doi.org/10.1007/s11207-009-9367-0

Mason, G. M., Leske, R. A., Desai, M. I., Cohen, C. M. S., Dwyer, J. R., Mazur, J. E., et al. (2008). Abundances and energy spectra of corotating interaction region heavy ions observed during solar cycle 23. *The Astrophysical Journal*, *678*, 1458. https://doi.org/10.1086/533524

Mason, G. M., Mazur, J. E., Dwyer, J. R., Reames, D. V., & von Rosenvinge, T. T. (1997). New spectral and abundance features of interplanetary heavy ions in corotating interaction regions. *Acta Pathologica Japonica*, *486*, L149. https://doi.org/10.1086/310845

Mason, G. M., & Sanderson, T. R. (1999). CIR associated energetic particles in the inner middle heliosphere. *Space Science Reviews*, *89*, 77–90. https://doi.org/10.1023/A:1005216516443

McComas, D. J., Alexander, N., Angold, N., Bale, S., Beebe, C., Birdwell, B., et al. (2016). Integrated Science Investigation of the Sun (ISIS): Design of the energetic particle investigation. *Space Science Reviews*, *204*, 187–256. https://doi.org/10.1007/s11214-014-0059-1

McComas, D. J., Christian, E. R., Cohen, C. M. S., Cummings, A. C., Davis, A. J., Desai, M. I., et al. (2019). Probing the energetic particle environment near the Sun. *Nature*, *576*, 223–227. https://doi.org/10.1038/s41586-019-1811-1

Müller-Mellin, R., Böttcher, S., Falenski, J., Rode, E., Duvet, L., Sanderson, T., et al. (2008). The solar electron and proton telescope for the STEREO mission. *Space Science Reviews*, *136*, 363–389. https://doi.org/10.1007/s11214-007-9204-4

Murphy, N., Smith, E. J., & Schwadron, N. A. (2002). Stronly underwound magnetic fields in co-rotating rarefaction regions: Observations and implications. *Geophysical Research Letters*, *29*(22), 2066. https://doi.org/10.1029/2002GL015164

Ogilvie, K. W., Chornay, D. J., Frizenreiter, R. J., Hunsaker, F., Keller, J., Lobell, J., et al. (1995). SWE: A comprehensive plasma instrument for the wind spacecraft. *Space Science Reviews*, *71*, 55–77. https://doi.org/10.1007/BF00751326

Pizzo, V. (1978). A three-dimension model of corotating streams in the solar wind 1. Theoretical foundations. *Journal of Geophysical Research*, *83*, 5563–5572. https://doi.org/10.1029/JA083iA12p05563

Richardson, I. G. (1985). Low energy ions in co-rotating interaction regions at 1 AU: Evidence for statical ion acceleration. *Planetary and Space Science*, *33*, 557–569. https://doi.org/10.1016/0032-0633(85)90097-2l

Richardson, I. G. (2018). Solar wind stream interaction regions throughout the heliosphere. *Living Reviews in Solar Physics*, *15*, 1. https://doi.org/10.1007/s41116-017-0011-z

Richter, A. K., & Luttrell, A. H. (1986). Superposed epoch analysis of corotating interaction regions at 0.3 and 1.0 AU: A comparative study. *Journal of Geophysical Research: Space Physics*, *91*(A5), 5873–5878. https://doi.org/10.1029/JA091iA05p05873

Schwadron, N. A. (2002). An explanation for strongly underwound magnetic field in co-rotating rarefaction regions and its relationship to footpoint motion on the sun. *Geophysical Research Letters*, *29*(14), 1663. https://doi.org/10.1029/2002GL015028

Schwadron, N. A., Fisk, L. A., & Gloackler, G. (1996). Statistical acceleration of interstellar pick-up ions in co-rotating interaction regions. *Geophysical Research Letters*, *23*, 2871–2874. https://doi.org/10.1029/96GL02833

Schwadron, N. A., Joyce, C. J., Aly, A., Cohen, C. M. S., Desai, M. I., Mccomas, D., et al. (2020). A new view of energetic particles from stream interaction regions observed by Parker Solar Probe. *Astronomy and Astrophysics*, https://doi.org/10.1051/0004-6361/202039352

Schwadron, N. A., & McComas, D. J. (2005). The sub-Parker spiral structure of the heliospheric magnetic field. *Geophysical Research Letters*, *32*, L03112. https://doi.org/10.1029/2004GL021579

Schwenn, R. (1990). Large-scale structure of the interplanetary medium. In R. Schwenn & E. Marsch (Eds.), *Physics of the inner heliosphere I. Physics and chemistry in space, space and solar phycis* (Vol. *20*). Berlin, Heidelberg: Springer. https://doi.org/10.1007/978-3-642-75361-9_3

Simnett, G. M., & Roelof, E. C. (1995). Reverse shock acceleration of electrons and protons at mid-heliolatitudes from 5.3-3.8 AU. *Space Science Reviews*, *72*, 303.

Smith, E. J., Tsurutani, B. T., & Rosenberg, R. L. (1978). Observations of the interplanetary sector structure up to heliographic latitudes of 16°: Pioneer 11. *Journal of Geophysical Research*, *83*, 717–724. https://doi.org/10.1029/JA083iA02p00717

Smith, E. J., & Wolfe, J. H. (1976). Observations of interaction regions and corotating shocks between one and five AU: Pioneers 10 and 11. *Geophysical Research Letters*, *3*, 137–140. https://doi.org/10.1029/GL003i003p00137

Tsurutani, B. T., Smith, E. J., Pyle, K. R., & Simpson, J. A. (1982). Energetic protons accelerated by corotating shocks: Pioneer 10 and 11 observations from 1 to 6 AU. *Journal of Geophysical Research*, *87*, 7389–7404. https://doi.org/10.1029/JA087iA09p07389

Van Hollebeke, M. A. I., McDonald, F. B., Trainor, J. H., & Von Rosenvinge, T. T. (1981). coronating energetic particle and fast plasma streams in the inner and outer solar system—Radial dependence and energy spectra, solar wind 4. In *H. Rosenbauer (Ed.), Proceedings of the conference held in August 18-September 1, 1978 in Burghausen, FDR, MPAE-W-100-81-31* (pp. 497). Garching, FDR: Max-Planck-Institute für Aeronomie.

Wijsen, N., Aran, A., Pomoell, J., & Poedts, S. (2019). Interplanetary spread of solar energetic protons near a high-speed solar wind stream. *Astronomy and Astrophysics*, *624*, A47.

Zhao, L., Li, G., Ebert, R. W., Dayeh, M. A., Desai, M. I., Mason, G. M., et al. (2015). Modeling transport of energetic particles in corotating interaction regions: A case study. *Journal of Geophysical Research: Space Physics*, *121*, 77–92. https://doi.org/10.1002/2015JA021762